ARTICLES
PUBLISHED ONLINE: 11 JULY 2016 | DOI: 10.1038/NPHYS3810
nature physics

Time reversal and holography with spacetime transformations

Vincent Bacot[1], Matthieu Labousse[1,2†], Antonin Eddi[3], Mathias Fink[1*‡] and Emmanuel Fort[1*‡]

Wave control is usually performed by spatially engineering the properties of a medium. Because time and space play similar roles in wave propagation, manipulating time boundaries provides a complementary approach. Here, we experimentally demonstrate the relevance of this concept by introducing instantaneous time mirrors. We show with water waves that a sudden change of the effective gravity generates time-reversed waves that refocus at the source. We generalize this concept for all kinds of waves, introducing a universal framework which explains the effect of any time disruption on wave propagation. We show that sudden changes of the medium properties generate instant wave sources that emerge instantaneously from the entire space at the time disruption. The time-reversed waves originate from these 'Cauchy sources', which are the counterpart of Huygens virtual sources on a time boundary. It allows us to revisit the holographic method and introduce a new approach for wave control.

Holographic methods are based on the time-reversal invariance of wave equations. They rely on the fact that any wave field can be completely determined within a volume by knowing the field (and its normal derivative) on any enclosing surface[1,2]. Hence, information reaching the two-dimensional (2D) surface is sufficient to recover all information inside the whole volume. Based on these properties, Denis Gabor introduced the holographic method, which provides an elegant way to back-propagate a monochromatic wave field and obtain 3D images. More recently, time-reversal mirrors exploited the same principles extended to a broadband spectrum to create time-reversed waves. This latter approach has been implemented with acoustic[3,4], elastic[5], electromagnetic[6] and water waves[7,8]. It requires the use of emitter–receptor antennas positioned on an arbitrary enclosing surface. The wave is recorded, digitized, stored, time-reversed and rebroadcast by the antenna array. If the array intercepts the entire forward-propagating wave with a good spatial sampling, it generates a perfect backward-propagating copy. Note that this process is difficult to implement in optics[9,10], and the standard solution is to work with monochromatic light and use nonlinear regimes such as three-wave or four-wave mixing[11,12].

Here, within the general concept of spacetime transformations[13–16], we completely revisit the holographic method and introduce a new way to create wideband time-reversed wave fields in 2D or 3D by manipulating time boundaries. Time boundaries have recently received much attention because they have been shown to play a major role in several phenomena, such as time refraction, the dynamic Casimir effect, Hawking radiation, photon acceleration and self-phase modulation[17–26]. In addition, different suggestions to process wideband time reversal have been proposed in optics to associate both time and spatial modulation of the medium refractive index. These suggestions, mainly for 1D propagation, rely on a dynamic tuning of photonic crystals and metamaterials[27,28].

Our approach is related to the Cauchy theorem, which states that the wave field evolution can be deduced from the knowledge of this wave field (and its time derivative) at one single time (the so-called initial conditions)[29]. It is the dual time equivalent of standard time reversal based on spatial boundaries. We use a sudden modification of the wave propagation properties of the medium to create a time-reversed wave. This time disruption realizes an instantaneous time mirror (ITM) in the entire space without the use of any antenna or memory. The information stored in the whole medium at one instant plays the role of a bank of memories.

We will subsequently introduce the concept of the ITM and show its first experimental demonstration. The experiment is spectacular because it is conducted with water waves and can therefore be observed with the naked eye. We first interpret the backward wave propagation in the ITM as an emission by isotropic sources created during the time disruption. These 'Cauchy sources' define a new set of initial conditions for the wave field propagation after the ITM, allowing us to revisit the Huygens–Fresnel principle. We then discuss this experiment in terms of time discontinuities and conservation laws. Finally, we analyse the spacetime symmetries of ITMs compared to standard mirrors.

In the nineteenth century, Loschmidt challenged Boltzmann's attempt to describe irreversible macroscopic processes with reversible microscopic equations[30,31]. He imagined a daemon capable of instantaneously reversing all velocities of all particles in a gas. Such an operation can be ascribed to a change in initial conditions resulting in a time-reversed motion of all particles that would return to their initial positions. The extreme sensitivity to initial conditions that lies at the heart of chaotic phenomena in nonlinear dynamics renders any such particulate scheme impossible. Waves are more amenable, because they can be described in many situations by a linear operator, and any error in initial conditions will not suffer from chaotic behaviour. The wave analogue of this Loschmidt daemon is related to the Cauchy

[1]Institut Langevin, ESPCI, CNRS, PSL Research University, 1 rue Jussieu, 75005 Paris, France. [2]Matière et Systèmes Complexes, Université Paris Diderot, CNRS 7057, Sorbonne Paris Cité, 10 Rue A. Domon et L. Duquet, 75013 Paris, France. [3]Laboratoire de Physique et Mécanique des Milieux Hétérogènes, ESPCI, CNRS, PSL Research University, 10 rue Vauquelin, 75005 Paris, France. †Present address: Laboratoire Matériaux et Phénomènes Quantiques, Université Paris Diderot, Sorbonne Paris Cité, 10 rue A. Domon et L. Duquet, 75013 Paris, France. ‡These authors contributed equally to this work.
*e-mail: mathias.fink@espci.fr; emmanuel.fort@espci.fr

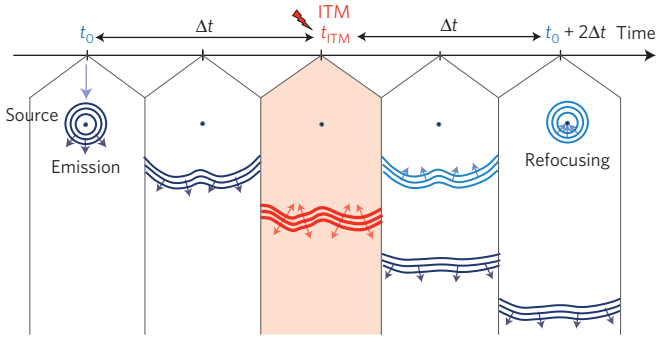

Figure 1 | Schematic of the instantaneous time mirror. A wave source emits at time t_0 a wavepacket which propagates in a given medium. A sudden spatially homogeneous disruption of the wave propagation properties occurs in the entire medium at time $t_{ITM} = t_0 + \Delta t$. It results in the production of a counter-propagating time-reversed wave in addition to the initial forward-propagating wave. The counter-propagating wave refocuses at the source position at time $t_0 + 2\Delta t$.

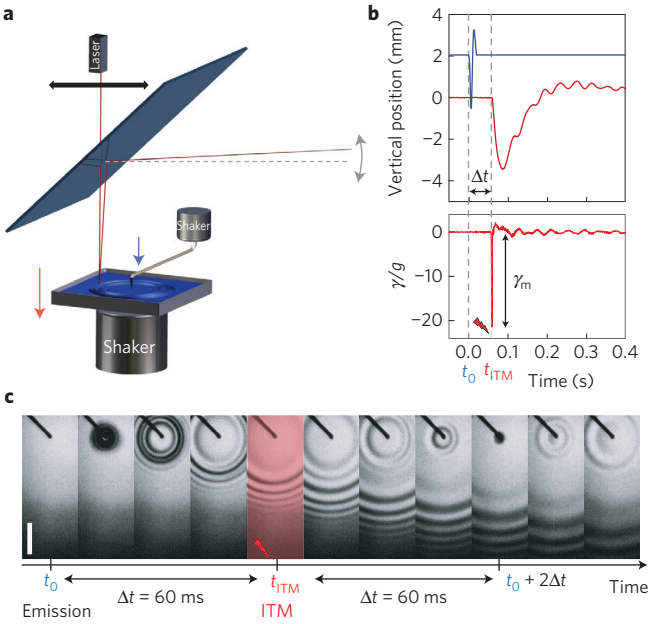

Figure 2 | ITM experimental implementation. a, Experimental set-up. A bath of water is placed on a shaker to apply a vertical jolt. Another shaker is used to hit the water surface with a tip to generate surface waves. The deflection of a laser beam is used to measure the local surface slope. The laser is placed on a computer-controlled translation device to scan the surface. **b**, Typical time variations of the vertical position of the emitter (a tip) in blue and of the bath (in red) together with the bath acceleration γ in an ITM experiment. γ_m is the maximum downward acceleration. Δt is the time delay between the wave emission and the jolt. **c**, Image sequence of an ITM experiment (top view) with a point source, showing the divergent wave and the time-reversed wave which diverges again after focusing back at the source position. $\gamma_m = -21g$ and $\Delta t = 60$ ms. Scale bar, 1 cm (see Supplementary Video 1).

theorem. The latter states that the future evolution of any wave field $\phi(\boldsymbol{r},t)$ at position $\boldsymbol{r}$ and time t can be inferred from the knowledge of the set of initial conditions $(\phi, \partial\phi/\partial t)_{t_m}$, with the field amplitude $\phi(\boldsymbol{r},t_m)$ and time derivative $\partial\phi/\partial t(\boldsymbol{r},t_m)$ at a given time t_m, in the whole space. The analogue of the particle velocity reversal is to take the new set of initial conditions $(\phi, -(\partial\phi/\partial t))_{t_m}$ that causes a time-reversed wave whose time dependence is inverted. However, because of the wave superposition principle, the emergence of this time-reversed wave is not limited to this choice of initial conditions. For instance, the new initial condition $(\phi, 0)_{t_m}$ can be split into $1/2(\phi, \partial\phi/\partial t)_{t_m}$ associated with a forward wave and $1/2(\phi, -(\partial\phi/\partial t))_{t_m}$ associated with a backward time-reversed wave. This particular choice erases the arrow of time by starting from a 'frozen' picture of the wave field at time t_m with no favoured direction of propagation. Similarly, a new set of initial conditions $(0, \partial\phi/\partial t)_{t_m}$ in which the wave field is null would also comprise a backward-propagating wave with a negative sign. More generally, the superposition of backward- and forward-propagating waves results from the decoupling of the wave field from its time derivative at a given time (see Fig. 1 and the Supplementary Information). Because both are bound together by the wave celerity, its disruption can lead to such decoupling. This offers a straightforward way to experimentally implement an ITM.

In this study, we use gravity–capillary waves to implement the concept of ITMs. Because the surface wave celerity depends on the effective gravity, the disruption of the celerity is achieved by applying a vertical jolt to the whole liquid bath. Figure 2a shows the experimental set-up. A bath of water is placed on a shaker to control its vertical motion. A plastic tip fixed on another shaker is used to hit the liquid surface and generate a point source of waves at time $t_0 = 0$. Figure 2b shows a typical time sequence of the vertical tip and bath motions used to generate the surface waves and implement the ITM. An image sequence of the wave propagation on the bath taken from above is shown in Fig. 2c. A circular wavepacket centred on the impact point is emitted as the tip hits the surface. The average wave propagation velocity is of the order of magnitude of 10 cm s^{-1}. After time $t_{ITM} = 60$ ms, a vertical downward jolt is applied to the bath. The bath acceleration reaches $\gamma_m = -21g$ in approximately 2 ms. The propagation of the initial outward-propagating wave is not qualitatively affected by this disruption. However, at the time of the disruption, we observe the appearance of a backward-converging circular wavepacket that diverges again upon passing through the original impact point source.

Figure 3a is a time sequence of the profile of a wavepacket propagating originally from left to right. The wavelength spreading induced by dispersion is clearly visible. The ITM generates a time-reversed wavepacket propagating in the opposite direction. The resulting surface profile can be decomposed into the propagating and counter-propagating wavepackets using Fourier analysis. We observe that the shape of the backward wavepacket is very similar to that of the initial wavepacket. Both profiles almost superimpose in shape and position when measured at symmetrical times Δt from the ITM. A phase shift of approximately $\pi/2$ is observed between the forward and backward wavepackets at the time of the ITM. In contrast with standard reflection, the backward wavepacket is not spatially reversed. The time-reversed nature of the backward wave allows the wavepacket to compensate for dispersion. The fast short wavelengths will catch up with the slow long wavelengths, thus refocusing the wavepacket. Its amplitude depends linearly on the vertical acceleration of the bath (Fig. 3b). The ITM is a broadband time-reversal mirror. The time-reversed spectrum is independent of the jolt amplitude and is nearly identical to that of the initial wave (Fig. 3c). Note that, after the ITM, the high frequencies of the time-reversed waves are damped during the refocusing process, due to the viscosity of water (see Fig. 3a).

Figure 4 shows two examples of ITMs performed on sources with complex source shapes. In both cases, the ITM disruption occurs long after the wave field has lost any resemblance to its initial shape at the time of emission. The refocussing back to its initial shape indicates the time-reversal nature of the process.

We now focus on the underlying principles of ITMs. ITMs are implemented through a wave celerity disruption induced by the gravity jolt. For the sake of generality, let us consider waves governed by d'Alembert's wave equation. We introduce a time-dependent

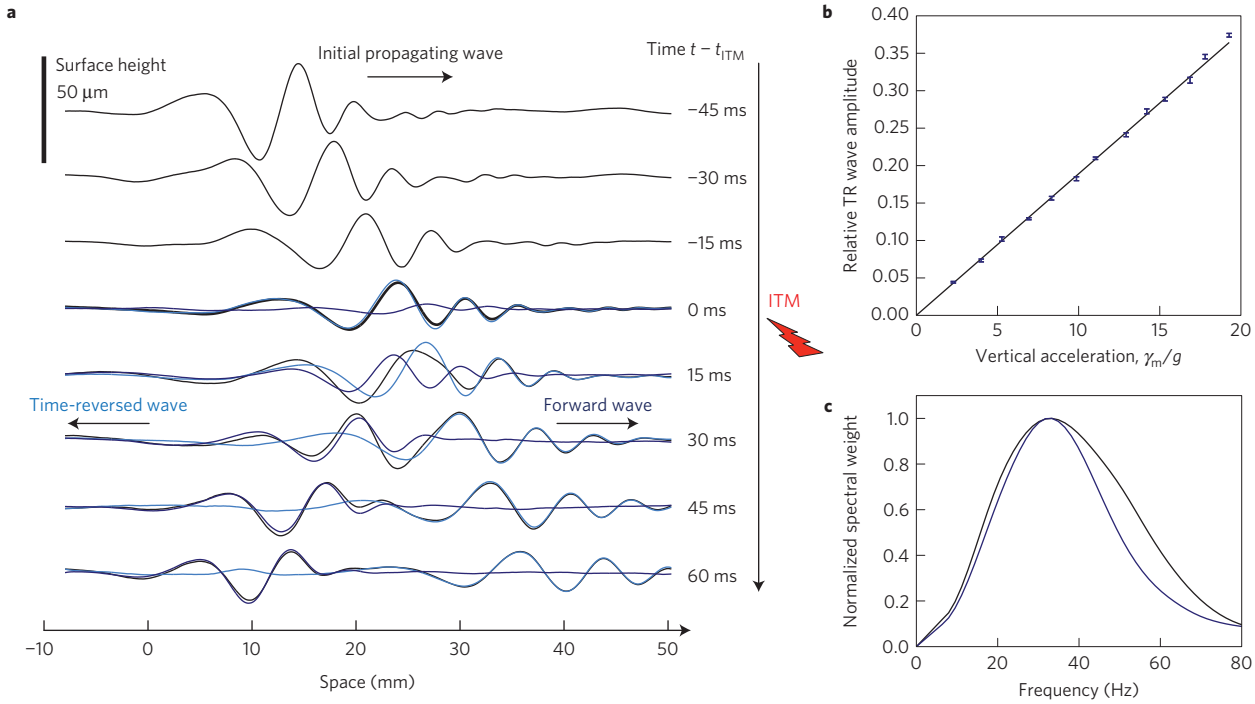

Figure 3 | ITM on a wavepacket. a, Evolution of the profile of a wavepacket produced by a point source and later subjected to an ITM (see Supplementary Video 2). The surface height (black solid line) is obtained by integrating slope measurements carried out on a line going through the emission point (see Fig. 1 and Supplementary Video 1). To the original wavepacket propagating from left to right, a time-reversed one propagating from right to left is added as the ITM occurs. The two counter-propagating components of the surface profile are separated using Fourier analysis: the dark blue line represents the ongoing forward wave while the light blue line represents the time-reversed wave. **b**, Relative amplitude of the time-reversed wave normalized by the forward wave amplitude as a function of the jolt amplitude. The measurement is performed in water at 1.6 cm from the point source. The ITM is applied with a time delay of $\Delta t = 170$ ms. The solid line is a linear fit which is coherent with the theory (see Supplementary Information). The error bar represents the standard deviation obtained from a series of ten measurements. **c**, Normalized spectra of the time-reversed wavepacket (light blue) and of the initial forward wavepacket (dark blue). Both are similar, with respective maximum frequency $\omega_{max} \approx 35$ Hz and full-width at half-maximum $\Delta\omega \approx 35$ Hz.

phase velocity $c(t) = c_0/n(t)$, where $n(t)$ is a time-dependent index and c_0 is the phase velocity in the absence of the ITM. The disruption undergone by the medium in an ITM can be modelled by a δ-Dirac function such that $c(t)^2 = c_0^2(1 + \alpha\delta(t - t_{ITM}))$. The wave equation can be written as a nonhomogeneous equation in which the equivalent source term $s(\boldsymbol{r}, t)$ is induced by the velocity disruption (see Supplementary Information):

$$\Delta\phi(\boldsymbol{r}, t) - \frac{1}{c_0^2}\frac{\partial^2\phi}{\partial t^2}(\boldsymbol{r}, t) = s(\boldsymbol{r}, t) \qquad (1)$$

with $s(\boldsymbol{r}, t) = -(\alpha/c_0^2)\delta(t - t_{ITM})(\partial^2\phi/\partial t^2)(\boldsymbol{r}, t)$.

The source term is localized in time but delocalized in space. It corresponds to an instantaneous source that is proportional to the second time derivative of the wave field at the instant t_{ITM} of the disruption. Equation (1) can also be applied in the Fourier domain to water waves to take account of dispersion. All the results subsequently presented for d'Alembert waves can thus be recovered for water waves (see Supplementary Information). Considering both the specific dispersion relation of these waves and the experimental profile of the jolt, we used equation (1) to simulate ITM action in our experiments (see Supplementary Information).

This description with a source term allows us to revisit the Huygens–Fresnel theory. To model the wave propagation, Huygens hypothesized that every point on a wavefront emits secondary spherical wavelets[32]. The wavefront at any later time $t + \Delta t$ conforms to the upper envelope of the wavelets emanating from every point on the wavefront at a prior instant t (Fig. 5a). However, neglecting the backward-propagating envelope was arbitrary. Only later did Fresnel[33], followed by Kirchhoff[34], prove that the wavelets interfere destructively in the backward direction and maintain the expected forward propagation, by adding a dipolar component to the secondary sources.

In our experiment, the temporal disruption modifies the classical interplay between the dipolar and monopolar sources that causes a propagating wave. It suddenly creates real monopolar sources $s(\boldsymbol{r}, t)$ instantaneously in the whole space (see equation (1)). These sources radiate isotropically, generating an additional wave field, both forward and backward (see Fig. 5a). Because they modify the initial conditions of the wave field on a time boundary, these sources can be termed Cauchy sources.

What is the relation between these Cauchy sources and the change of initial conditions induced by an ITM? Just before the ITM at t_{ITM}^-, the wave field is $(\phi, \partial\phi/\partial t)_{t_{ITM}^-}$. It is modified by the disruption into $(\phi, \partial\phi/\partial t)_{t_{ITM}^+}$ just after the ITM at t_{ITM}^+. The new initial state is given by (see Supplementary Information):

$$\left(\phi, \frac{\partial\phi}{\partial t}\right)_{t_{ITM}^+} = \left(\phi(\boldsymbol{r}, t_{ITM}^-), \frac{\partial\phi}{\partial t}(\boldsymbol{r}, t_{ITM}^-) + \alpha\frac{\partial^2\phi}{\partial t^2}(\boldsymbol{r}, t_{ITM}^-)\right) \qquad (2)$$

This new initial state can be decomposed as previously discussed, by using the superposition principle, into the superposition of the original state of the unperturbed wave field $(\phi, \partial\phi/\partial t)_{t_{ITM}^-}$ plus an added state $(0, \alpha(\partial^2\phi/\partial t^2))_{t_{ITM}^-}$. This latter term can again be decomposed into two states: $\alpha/2(\partial\phi/\partial t, \partial^2\phi/\partial t^2)_{t_{ITM}^-}$ and $-(\alpha/2)(\partial\phi/\partial t, -(\partial^2\phi/\partial t^2))_{t_{ITM}^-}$, which correspond to a forward-propagating wave field and a time-reversed backward-propagating wave field, respectively. Both wave fields are proportional to the time derivative of the original incident wave field. Provided that

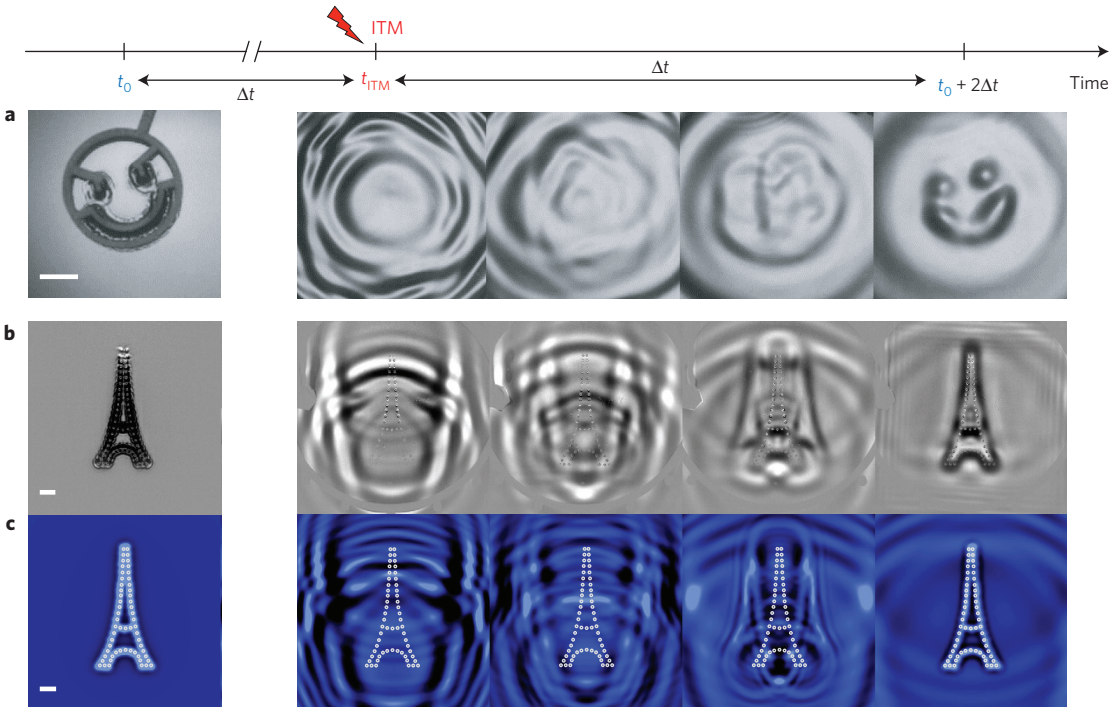

Figure 4 | Image sequence of the instantaneous time reversal of a complex wave field. a,**b**, Source composed of tips that hit the surface positioned in the shape of a Smiley (**a**; see Supplementary Video 3) or air blowing between two sealed Plexiglas plates placed at 1 cm above the bath with holes positioned in the shape of an Eiffel tower (**b**; see Supplementary Video 4). In the sequence shown in **b**, the image without blowing has been subtracted as a reference. **c**, Numerical simulation of **b** using the ITM model for water waves and the experimental jolt profile (see Supplementary Information and Video 5). The images on the left show this emission process. At the instant of the ITM, the wave field features a complex interference pattern in which the original shape is no longer apparent. As the time-reversed wave refocuses, the shape of the source becomes visible again. Time interval between two successive images is 26 ms for **a** and 66 ms for **b** and **c**. Scale bars, 1 cm. White dots indicate the position of the sources in the simulation **c**.

the bandwidth of the time-reversed wave is not too large compared to the central frequency, these wave fields are proportional to the original wave field itself, as observed in the experiments. Note that the expected $\pi/2$ phase shift between the wave field and its derivative is the one observed in the experiment (see Fig. 3a). In practice, the time-reversed bandwidth is limited by that of the ITM disruption (see Fig. 3c), which should be non-adiabatic for wave propagation.

It is interesting to compare standard time-reversal mirrors (TRMs) and ITMs. In contrast with a standard TRM implementation, an ITM does not require the introduction of localized transducers, and thus does not introduce perturbative elements in the medium, spatial confinement or sampling issues to fulfil the Nyquist criteria. An ITM, however, requires strong non-adiabatic variations of the refractive index, which can be difficult to implement, for instance, in the case of light. For 1D and 2D wave control, nonlinear optics can induce instantaneous refractive index changes by taking advantage of the off-axis or off-plane dimensions. Phase transitions can also be used to enhance the amplitude of the refractive index change. Note that standard TRMs with digital recording are too slow to perform phase measurements for light frequencies. Whereas TRM performances are determined by the spectral response of the transducers, the limitation of ITMs is mainly associated with the characteristic time of the disruption. An ITM can be performed instantly at any time in the whole medium, whereas standard TRMs must be delayed. Note, however, that the use of digital memories enables more complex operations on the re-emitted signal (controlled delay, filtering,...), which proves interesting in several applications. In the ITM configuration, the time-reversed (TR) wave field is associated with the derivative of the initial wave field, as discussed previously (see Fig. 3a, see Supplementary Information). In the standard TRM, the TR wave field is associated with the antiderivative of the initial wave field[4]. In the case of relatively narrow band wavepackets, this leads respectively to an advanced or a retarded $\pi/2$ phase shift on the TR wave field. Note that this derivation or anti-derivation has no importance for TR applications and does not affect the refocusing.

ITMs can be analysed in the framework of time refraction[17–20]. The instantaneous time disruption for the wave speed can be considered as the limiting case of a rectangular time profile with two discontinuities: at time t_{ITM}^{-}, the wave speed jumps from c_0 to $c_1 = c_0/n_1$, and then at time t_{ITM}^{+}, changes back to its original value c_0. A temporal discontinuity in a homogeneous medium conserves the momentum but not the energy. In our experiment, this energy brought to the wave field is provided by the jolt. The time analogue of the Fresnel formula can be obtained from conservation laws[18,19]. Hence, a monochromatic wave $e^{i(\boldsymbol{k}\cdot\boldsymbol{r}-\omega_0 t)}$ of wavevector $\boldsymbol{k}$ and angular frequency ω_0 is split at the time discontinuity into a 'transmitted' wave $t_{01}e^{i(\boldsymbol{k}\cdot\boldsymbol{r}-\omega_1 t)}$ and a 'reflected' wave $r_{01}e^{i(\boldsymbol{k}\cdot\boldsymbol{r}+\omega_1 t)}$, where $\omega_1 = \omega_0/n_1$ is the angular frequency in medium 1, and t_{01} and r_{01} are temporal Fresnel coefficients for time refraction and reflection, respectively. Each wave emerging from the first temporal discontinuity will be split again into two waves at the second discontinuity (see Fig. 5b). This time slab is the time analogue of a Fabry–Pérot resonator. However, because of causality, multiple reflections are not permitted[18,19]. The time-reversed wave field is thus the result of interference between two backward waves with opposite signs (because $r_{01}t_{10} = -r_{10}t_{01}$). This explains why the resulting time-reversed field is not the perfect time reverse of the incident wave field ϕ, but rather of its derivative $\partial\phi/\partial t$, in the limiting case of an instant disruption (see the Supplementary Information).

We now focus on the spatio-temporal symmetries of ITMs using plane waves, without loss of generality. A standard 'spatial' mirror

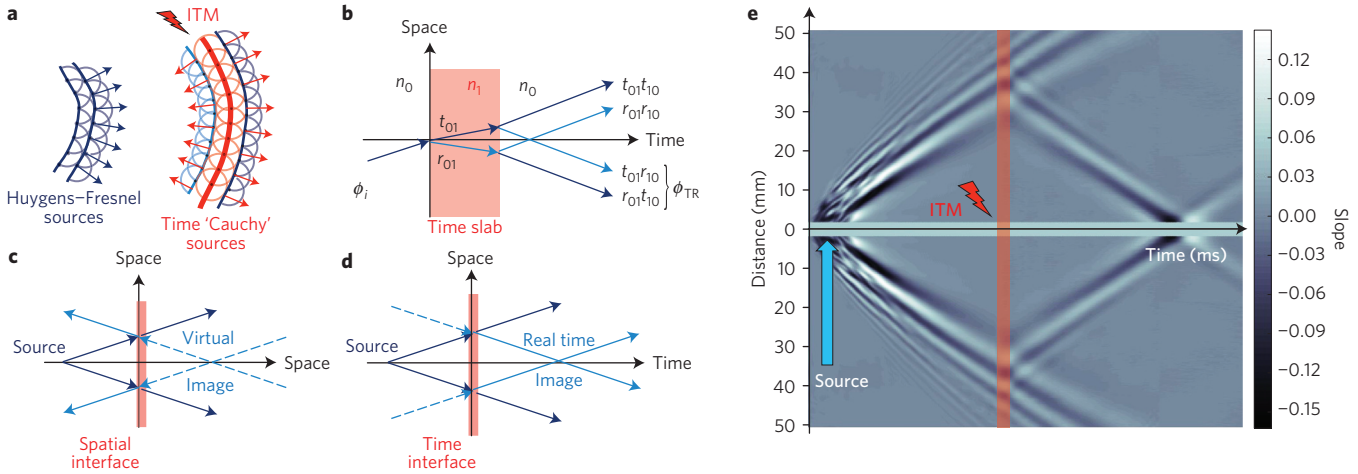

Figure 5 | The time equivalent of a mirror. a, Schematics comparing the standard wave propagation using secondary Huygens–Fresnel sources and the creation of real secondary 'Cauchy' sources during an ITM. **b**, Schematics of an incident wave field ϕ_i impinging on a time slab. ϕ_{TR} is the backward-propagating field. t_{ij} and r_{ij} are the transmission and reflection time Fresnel coefficients between medium i and j (see Supplementary Information). **c**,**d**, Schematics of a standard spatial mirror (**c**) and an instantaneous time mirror (**d**). These mirrors are the limit case of an infinitely thin space slab and an infinitely thin time slab, respectively (see Supplementary Information). The directions of the arrows show the spatio-temporal directions of wave propagation. With a standard mirror (**c**), the reflected beams are equivalent to those emitted by a virtual source situated at the symmetric point on the other side of the mirror. For the ITM (**d**), the image is situated at the symmetric instant to that of emission with respect to the time interface. Because of causality, this image is real, and corresponds to a focal point. **e**, Spatio-temporal diagram of the slope measurements in an ITM experiment with a point source (see Fig. 2c). The diagram is symmetrized for clarity. The area in red highlights the ITM disruption occurring after 80 ms with an approximate width of 8 ms. From this moment on, the time-reversed wave is observed. As it converges back to the emission point, this packet narrows down; the effect of dispersion being compensated.

(see schematic Fig. 5c) changes the sign of the wavevector normal component to its surface $k_\perp$. It changes the wave characteristics as $(k_\perp, k_\parallel, \omega) \rightarrow (-k_\perp, k_\parallel, \omega)$ by performing a space reversal in the normal direction. The incident wave $\phi(x, \ldots, t)$ becomes the reflected wave $\phi(2x_m - x, \ldots, t)$ for a mirror positioned along the x axis at x_m. For a point source, the reflected wave appear as though it is emitted from a virtual image located on the other side of the mirror. As previously mentioned, ITM symmetry is given by $(k_\perp, k_\parallel, \omega) \rightarrow (k_\perp, k_\parallel, -\omega)$. This corresponds to a time reversal: the incident wave $\phi(x, \ldots, t)$ becomes the time-reversed wave $\phi(x, \ldots, 2t_{ITM} - t)$ for an ITM at t_{ITM}. The direction of propagation for a plane wave is given by its phase $\boldsymbol{k} \cdot \boldsymbol{r} - \omega t$, which depends on the relative signs of $\boldsymbol{k}$ components and ω. Hence, in terms of symmetries, an ITM is equivalent to $(k_\perp, k_\parallel, \omega) \rightarrow (-k_\perp, -k_\parallel, \omega)$. Because all components of $\boldsymbol{k}$ are reversed, waves are backward-propagating. In the spacetime representation of the ITM (see Fig. 5d), the waves refocus at their emitter positions, but on the other time side of the mirror in the time domain. This can be observed directly in the experiment on the spatio-temporal graph of waves emitted from the point source undergoing an ITM (see Fig. 5e). Note that this transformation is also directly related to materials with a negative index. Time reversal and negative refraction have been shown to be intimately linked processes[35].

Manipulating the wave propagation from the time boundaries offers a new approach to control and manipulate wave propagation. Time disruptions create instantaneous time mirrors acting simultaneously in the entire space and without the use of external emitters. This approach will be generalized to create dynamic control of the spatio-temporal boundaries of the medium. Water waves present unique advantages for implementation and visualization. In this perspective, several possibilities of precise and rapid spatio-temporal wave control are offered, for instance, by using ultrasound or electrostatic forces on the liquid surface. In the future, we intend to use these concepts of spacetime transformation to perform water-wave time cloaking and to revisit Faraday instability as a periodic time Bragg mirror. From this new perspective, we will experimentally address fundamental issues such as the dynamic Casimir effect.

Data availability

The data that support the plots within this paper and other findings of this study are available from the corresponding author upon request.

Received 23 September 2015; accepted 31 May 2016; published online 11 July 2016

References

1. Gabor, D. A new microscopic principle. *Nature* **161,** 777–778 (1948).
2. Bojarski, N. A survey of the near-field far-field inverse scattering inverse source integral equation. *IEEE Trans. Antenna Propag.* **30,** 975–979 (1982).
3. Fink, M. Time reversal of ultrasonic fields. I. Basic principles. *IEEE Trans. Ultrason. Ferroelectr. Freq. Control.* **39,** 555–66 (1992).
4. Fink, M. Time-reversal waves and super resolution. *J. Phys.* **124,** 012004 (2008).
5. Draeger, C. & Fink, M. One-channel time reversal of elastic waves in a chaotic 2D-silicon cavity. *Phys. Rev. Lett.* **79,** 407–410 (1997).
6. Lerosey, G. *et al*. Time reversal of electromagnetic waves. *Phys. Rev. Lett.* **92,** 193904 (2004).
7. Przadka, A. *et al*. Time reversal of water waves. *Phys. Rev. Lett.* **109,** 064501 (2012).
8. Chabchoub, A. & Fink, M. Time-reversal generation of rogue waves. *Phys. Rev. Lett.* **112,** 124101 (2014).
9. Aulbach, J., Gjonaj, B., Johnson, P. M., Mosk, A. P. & Lagendijk, A. Control of light transmission through opaque scattering media in space and time. *Phys. Rev. Lett.* **106,** 103901 (2011).
10. Katz, O., Small, E., Bromberg, Y. & Silberberg, Y. Focusing and compression of ultrashort pulses through scattering media. *Nature Photon.* **5,** 372–377 (2011).
11. Yariv, A. Four wave nonlinear optical mixing as real time holography. *Opt. Commun.* **25,** 23–25 (1978).
12. Miller, D. A. B. Time reversal of optical pulses by four-wave mixing. *Opt. Lett.* **5,** 300–302 (1980).
13. Leonhardt, U. Optical conformal mapping. *Science* **312,** 1777–1780 (2006).
14. Pendry, J. B., Schurig, D. & Smith, D. R. Controlling electromagnetic fields. *Science* **312,** 1780–1782 (2006).
15. Cai, W. S., Chettiar, U. K., Kildishev, A. V. & Shalaev, V. M. Optical cloaking with metamaterials. *Nature Photon.* **1,** 224–227 (2007).

16. Chen, H., Chan, C. T. & Sheng, P. Transformation optics and metamaterials. *Nature Mater.* **9,** 387–396 (2010).
17. Mendonça, J. T. & Shukla, P. K. Time refraction and time reflection: two basic concepts. *Phys. Scripta* **65,** 160–163 (2002).
18. Mendonça, J. T., Martins, A. M. & Guerreiro, A. Temporal beam splitter and temporal interference. *Phys. Rev. A* **68,** 043801 (2003).
19. Salem, M. A. & Caloz, C. Space-time cross-mapping and application to wave scattering. Preprint at http://arXiv.org/abs/1504.02012 (2015).
20. Xiao, Y., Maywar, D. N. & Agrawal, G. P. Reflection and transmission of electromagnetic waves at a temporal boundary. *Opt. Lett.* **39,** 574–577 (2014).
21. Jaskula, J.-C. *et al*. Acoustic analog to the dynamical Casimir effect in a Bose–Einstein condensate. *Phys. Rev. Lett.* **109,** 220401 (2012).
22. Mendonça, J. T., Tito, J., Brodin, G. & Marklund, M. Vacuum effects in a vibrating cavity: time refraction, dynamical Casimir effect, and effective Unruh acceleration. *Phys. Lett. A* **372,** 5621–5624 (2008).
23. Mendonça, J. T. *Theory of Photon Acceleration* (CRC Press, 2000).
24. Alfano, R. R. *The Supercontinuum Laser Source* (Springer, 1989).
25. Wilson, C. M. *et al*. Observation of the dynamical Casimir effect in a superconducting circuit. *Nature* **479,** 376–379 (2011).
26. Shaltout, A., Kildishev, A. & Shalaev, V. Time-varying metasurfaces and Lorentz non-reciprocity. *Opt. Mater. Express* **5,** 2459–2467 (2015).
27. Chumak, A. V. *et al*. All-linear time reversal by a dynamic artificial crystal. *Nature Commun.* **1,** 141 (2010).
28. Sivan, Y. & Pendry, J. B. Time-reversal in dynamically-tuned zero-gap periodic systems. *Phys. Rev. Lett.* **106,** 193902 (2011).
29. Hadamard, J. *Lectures on Cauchy's Problem in Linear Partial Differential Equations* (Dover Phoenix editions, Dover Publications, 2003).
30. Loschmidt, J. Über den Zustand des Wärmegleichgewichts eines Systems von Körpern mit Rücksicht auf die Schwerkraft. *Sitz. Akad. Wiss. Wien* **2,** 128–142 (1876).
31. Jalabert, R. & Pastawski, H. Environment-independent decoherence rate in classically chaotic systems. *Phys. Rev. Lett.* **86,** 2490–2493 (2001).
32. Huygens, Chr. *Traitè de la Lumière* (Leyden, 1690), English translation by SP Thompson, Treatise on Light (Macmillan, 1912).
33. Fresnel, A. Mémoire sur la diffraction de la lumière. *Ann. Chim. Phys.* **2,** 239–281 (1816).
34. Kirchhoff, G. Zur Theorie der Lichtstrahlen. *Ann. Phys.* **254,** 663–695 (1883).
35. Pendry, J. B. Time reversal and negative refraction. *Science* **322,** 71–73 (2008).

Acknowledgements

We are grateful to Y. Couder and S. Perrard for fruitful and stimulating discussions. We thank A. Souilah and X. Benoit-Gonin for their help in building the experimental set-up. The authors acknowledge the support of the AXA research fund and LABEX WIFI (Laboratory of Excellence ANR-10-LABX-24) within the French Program 'Investments for the Future' under reference ANR-10-IDEX-0001-02 PSL*.

Author contributions

All the authors discussed, interpreted the results and conceived the theoretical framework. M.F. and E.F. conceived the initial concept. V.B., A.E., M.F. and E.F. designed the experiment. V.B. and A.E. performed the experiments. M.L. extended the model to water waves and designed the simulations. V.B., M.F. and E.F. wrote the paper. All authors reviewed the manuscript.

Additional information

Supplementary information is available in the online version of the paper. Reprints and permissions information is available online at www.nature.com/reprints. Correspondence and requests for materials should be addressed to M.F. or E.F.

Competing financial interests

The authors declare no competing financial interests.